SMART CEMENT MODIFIED WITH NANOPARTICLES FOR SENSING, RESISTANCE TO CONTAMINATION AND REAL TIME MONITORING OF INSTALLATION OF OIL WELLS WITH SIMULATED PHYSICAL MODEL TESTS

C. Vipulanandan Ph.D., P.E.
Center for Innovative Grouting Material and Technology (CIGMAT)
Department of Civil and Environmental Engineering
University of Houston, Houston, Texas 77204-4003

Abstract: Better controls during well drilling and cementing operation are critical to ensure safety during construction and the entire service life of the wells. For a successful cementing operation determine the setting of cement in place length of cement supporting the casing and performance of the cement after hardening. At present there are no technologies available to monitor the cementing operations without using buried sensors that could weaken the cement sheath.

In this study, smart cement was modified with nanoparticles (iron (NanoFe) and calcium carbonate) to have better sensing and contamination resistive properties, so that its behavior can be monitored at various stages of construction and during the service life of wells. A series of experiments evaluated the smart cement behavior with and without nanoparticle in order to identify the most reliable sensing properties that can also be relatively easily monitored. Tests were performed on the smart cement from the time of mixing to hardened state behavior. During the initial setting the electrical resistivity changed with time based on the amount of NanoFe used to modify smart oil well cement. A new quantification concept has been developed to characterize cement curing based on electrical resistivity changes in the first 24 hours of curing. When cement was modified with 0.1 percent of conductive filer (CF), the piezoresistive behavior of the hardened smart cement was substantially improved without affecting the rheological and setting properties of the cement. For the smart cement the resistivity change at peak stress was about 2000 times higher than the change in the compressive strain after 28 days of curing. Additional of 1 percent NanoFe reduced the initial resistivity of the smart cement by 16 percent. In a 24-hour period the maximum change in the electrical resistivity (RI24hr) for the smart cement without NanoFe was 333 percent. The RI24hr for the smart cement with NanoFe increased with the amount of NanoFe. Addition of 1 percent NanoFe increased the compressive strength of the smart cement by 26 percent and 42 percent after 1 day and 28 days of curing respectively. The test results showed that NanoFe decreased the electrical resistivity of the smart cement slurries with and without NanoFe. For the smart cement modified with NanoFe, the resistivity change at peak stress was over 2800 times higher than the change in the compressive strain. A linear correlation was obtained between the RI24hr and the compressive strength of the modified smart cement based on the curing time. In this study, the effect of adding 1percent of nano $CaCO_3$ (NCC) on the smart cement was investigated in order to protect the smart cement against oil based mad (OBM) contamination. Several tests were performed to monitor the changes of the smart cement behavior with 3% OBM contamination and also how NCC can improve the properties of the contaminated smart cement. Variation of electrical resistivity of the smart cement with curing time was monitored from the initial time of mixing to 28 days

of curing under water. Adding 1 percent NCC to the smart cement reduced the initial resistivity from 1.07 Ω.m to 0.85 Ω.m, a 21% reduction but increased the compressive strength by over 50%. Also addition of nano CaCO3 increased the rheological properties of the cement. With 3% OBM contamination the viscosity of the cement slurries increased. Results showed that contamination of smart cement with OBM reduced the long term resistivity of the smart cement but adding NCC enhanced the electrical resistivity of the contaminated smart cement cured under water. The compressive strength of the smart cement contaminated with 3 percent of OBM decreased by 44% and 3% respectively after 1 day and 28 days of curing. Addition of NCC improved the compressive strength of the 3 percent OBM contaminated smart cement by 72% and 10% respectively after 1 day and 28 days of curing under water. In this study the electrical resistivity index (RI24) was used as an indicator for predict the compressive strength of the smart cement at various curing times. The relationships between RI24 and the compressive strength were linear for the smart cement with and without 1% NCC modification. In order to evaluate the piezoresistive behavior of the smart cement, 0.075 percent (BOWC) of conductive filer (CF) was added to the cement to enhance the piezoresistive behavior of the cement. Results showed that change in resistivity at compressive failure for the smart cement was over 1000 times more than compressive strain and addition of 1% NCC further enhanced it by about 37% after 1 day and 28% after 28 days of curing under water. The OBM contaminated smart cement showed less change in piezoresistivity at maximum compressive stress at failure than the smart cement but addition of 1% of NCC enhanced the piezoresistivity of OBM contaminated smart cement.

Also in this study, small physical oil well models were designed, built and used to demonstrate the concept of real time monitoring of the flow of smart drilling mud and smart cement and hardening of the cement sheath in place. Also a new method has been developed to monitor the electrical resistivity of the materials using the two probe method. Based on the test results it has been proven that resistivity dominates the behavior of drilling mud and smart cement. LCR meters (measures the inductance (L), capacitance (C) and resistance (R)) were used at 300 kHz frequency to measure the changes in resistance. Several laboratory scale model tests have been performed using instrumented casing with wires and thermo couples. When the drilling mud was in the model borehole the measured resistance was the highest based on the high resistivity of the drilling mud. Notable reduction in electrical resistance was observed with the flow of spacer fluid and cement. Change in the resistance of hardened cement has been continuously monitored up to about 100 days. The predicted and the measured electrical resistances of the hardening cement sheath outside the cemented casing agreed very well. Also the pressure testing showed the piezoresistive response of the hardened smart cement.

1. Introduction

Successful deepwater cementing requires minimum fluid loss with drilling mud and cement slurry unit weights compatible with the formation (Eoff et al. 2009; Griffith et al. 1997). There are number of challenges associated with installation of casings in deepwater. The challenges include low fracture gradients resulting from young unconsolidated sands and shallow drilling hazards such as shallow water flows or hydrate formations, bottom-hole temperature and pressure, rapidly varying geological formations, fluid loss and no real-time monitoring of the operations. Recent case studies in the Gulf of Mexico (GOM) have documented using specially formulated lightweight foamed cement slurry to avoid cement sheath damage caused by shallow-water flow.

Two separate studies performed on oil well blowouts in the U.S. coastal area, one done between the years of 1971 to 1991 and the other study was done during the period of 1992 to 2006, before the deepwater horizon blowout in the Gulf of Mexico in 2010. The two studies clearly identified cement failures as the major cause for blowouts [Izod et al. 2007]. Cementing failures increased significantly during the second period of study when 18 of the 39 blowouts were due to cementing problems [Izod et al. 2007]. Also the deep-water horizon blowout in the Gulf of Mexico in 2010, where there was eleven fatalities, was due to cementing issues [Carter et al. 2014]. With some of the reported failures and growing interest of environmental and economic concerns in the oil and gas industry, integrity of the cement sheath is of major importance. At present there is no technology available to monitor the cementing operation real time from the time of placement through the entire service life of the borehole. Also there is no reliable method to determine the length of the competent cement supporting the casing.

1.1 Theory and Concepts

It was very critical to identify the sensing properties for the cement and drilling mud that can be used to monitor the performance. After years of studies and based on the current study on oil well cements and drilling muds, electrical resistivity (□□□was selected as the sensing property for both cements and drilling muds. This makes it unique since same monitoring system can be used to evaluate the performance of the cement and drilling muds. Hence two parameters (resistivity and change in resistivity) will be used to quantify the sensing properties as follows:

$$R = \rho\ (L/A) = \rho\ K \tag{1}$$

Where, R = electrical resistance, L = Linear distance between the electrical resistance measuring points, A= effective cross sectional area, K = Calibration parameter is determined based on the resistance measurement method.

Normalized change in resistivity with the changing conditions can be represented as follows:

$$\Delta\rho/\rho = \Delta R/R \tag{2}$$

In resistivity of the materials (ρ) to changes (composition, curing, stress, fluid loss and temperature) has been quantified. Typical properties such as composition, curing, fluid loss and temperature are related to the resistivity (ρ) (Eqn. (1)). The change in resistivity ($\Delta\rho$) (Eqn. (2)) will support the monitoring of the changes in the material (cement and drilling mud/fluid) behavior.

Impedence Spectroscopy (IS) Model (Vipulanandan et al. 2013)

Equivalent Circuit

Identification of the most appropriate equivalent circuit to represent the electrical properties of a material is essential to further understand its properties. In this study, an equivalent circuit to represent the Smart Cement and Smart Drilling Mud was required for better characterization through the analyses of the IS data. There were many difficulties associated with choosing a correct equivalent circuit. It was necessary somehow to make a link between the different elements in the circuit and the different regions in the impedance data of the corresponding sample. Given the difficulties and uncertainties, approach is to use circuits which most appropriate from the expected behavior of the material under study.

In this study, different possible equivalent circuits were analyzed to find an appropriate equivalent circuit to represent the smart cement and drilling mud.

Case 1: General Bulk Material – Resistance and Capacitor

In the equivalent circuit for Case1, the contacts were connected in series, and both the contacts and the bulk material were represented using a capacitor and a resistor connected in parallel (Fig. 1).

In the equivalent circuit for Case 1, R_b and C_b are resistance and capacitance of the bulk material, respectively and R_c and C_c are resistance and capacitance of the contacts, respectively. Both contacts are represented with the same resistance (R_c) and capacitance (C_c) as they are identical. Total impedance of the equivalent circuit for Case 1 (Z_1) can be represented as follows:

$$Z_1(\sigma) = \frac{R_b(\sigma)}{1+\omega^2 R_b^2 C_b^2} + \frac{2R_c(\sigma)}{1+\omega^2 R_c^2 C_c^2} - j\left\{\frac{2\omega R_c^2 C_c(\sigma)}{1+\omega^2 R_c^2 C_c^2} + \frac{\omega R_b^2 C_b(\sigma)}{1+\omega^2 R_b^2 C_b^2}\right\}, \tag{3}$$

where ω is the angular frequency of the applied signal. When the frequency of the applied signal was very low, $\omega \rightarrow 0$, $Z_1 = R_b + 2R_c$, and when it is very high, $\omega \rightarrow \infty$, $Z_1 = 0$.

Case 2: Special Bulk Material - Resistance Only

In Case 2, as a special case of Case 1, the capacitance of the bulk material (C_b) was assumed to be negligible (Fig.2).

The total impedance of the equivalent circuit for Case 2 (Z_2) is as follows:

$$Z_2(\sigma) = R_b(\sigma) + \frac{2R_c(\sigma)}{1+\omega^2 R_c^2 C_c^2} - j\,\frac{2\omega R_c^2 C_c(\sigma)}{1+\omega^2 R_c^2 C_c^2}. \tag{4}$$

When the frequency of the applied signal was very low, $\omega \rightarrow 0$, $Z_2 = R_b + 2R_c$, and when it is very high, $\omega \rightarrow \infty$, $Z_2 = R_b$ (Fig. 3).

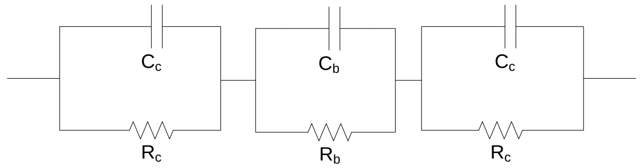

Figure 1. Equivalent circuit for Case1

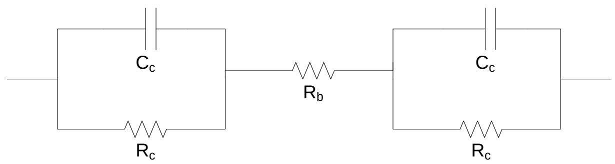

Figure 2. Equivalent circuit for Case 2

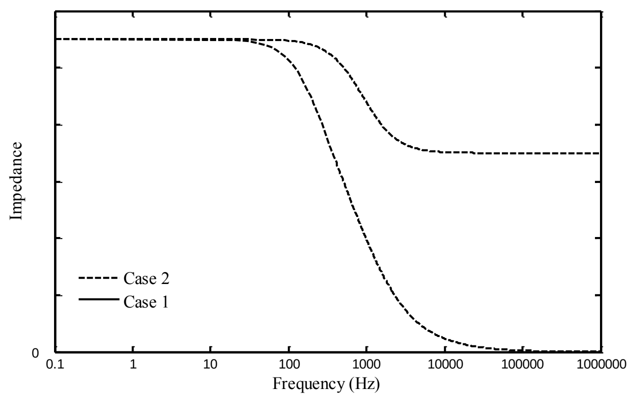

Figure 3. Comparison of typical responses of equivalent circuits for Case 1 and Case 2

Testing of smart cement, smart spacer fluid and smart drilling mud clearly indicated that Case 2 represented their behavior at a frequency of 300 kHz.

2. Objectives

The overall objective of this study was to investigate the effect of up to 1 percent of NanoFe on the modified smart cement (Class H) behavior. Rheological properties, compressive strength, and piezoresistive behavior were studied by monitoring the electrical resistivity.

The specific objectives were as follows:

i. Investigate the effect of nanoparticle in enhancing the sensing and contamination resistance properties of cement.
ii. Investigate the changes in the electrical resistivity during curing time of the smart cement.
iii. Compressive strength and piezoresistive behavior of the nanoparticle modified smart cement with and without oil based mud (OBM) contamination.

3. Materials and Methods

3.1 Cement

In this study commercially available Class H oil well cement was used.

(a) Sample Preparation

The samples were prepared in accordance with API standard. For the initial mixing, a high speed propeller-type mixer was used. Varying amounts of carbon fibers (0.075% to 0.2%) were added with the cement mix as base modification. Also various other additives were added with respect to the desired result. Additives were added to the water in the mixer with the mixing intervals of 20 s at 4000 rpm. Cement, water and additive were mixed at the speed of 4000 rpm for 3 min and 35 seconds at the speed of 1200 rpm. The water/cement ratio in all formulation in this study was varied from 0.38 to 0.44. Total of four wires were placed in the mold with two wires on each side of the specimen (Fig. 3). The vertical distances between any two wires were the same. Embedment depth of the conductive wire was 1 inch. In order to have consistent result, at least three specimens were prepared for each type of mix.

For setting time monitoring and compressive loading tests, cylinders with diameter of 2 inches and a height of 4 inches were prepared. For quick results monitoring, two-probe method was chosen. During the initial stages of setting, conductivity and API resistivity meters were used to determine the curing cement resistivity and using Eqn. (1) the calibration parameter K was obtained with time.

(b) Resistivity

Different instruments were used to measure the resistivity of the cement.

(i) Conductivity Probe: Commercially available conductivity probe was used to measure the conductivity (inverse of resistivity) of the fluids. In the case of cement, this meter was used during the initial curing of the cement. The conductivity measuring range was from 0.1 μS/cm to 1000 mS/cm representing a resistivity of 10,000 Ω.m to 0.1 Ω.m

(ii) Digital Resistivity Meter*:* This is used in the Petroleum industry to measure resistivity. It measures resistivity in the range of 0.01 Ω.m to 400 Ω.m.

(iii) Two Wire Method*:* The LCR Meter was used to measure the resistance between any two wires attached to the mold using AC at relatively high frequency. This configuration is first calibrated using the same liquid (cement slurry or drilling mud) to determine the parameter K in Eqn. (1). Typical variation of parameter K with time is shown in Fig. 4.

Testing of smart cement, smart spacer fluid and smart drilling mud clearly indicated that Case 2 represented their behavior at a frequency of 300 kHz.

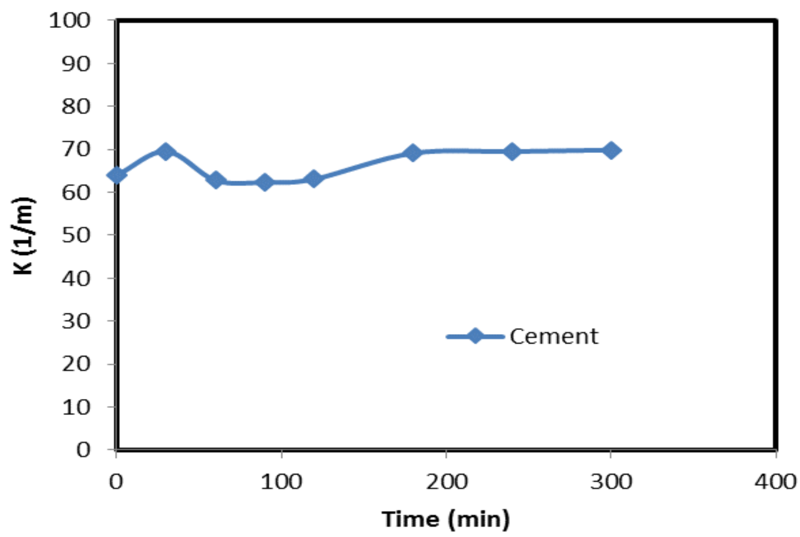

Figure 4. Typical Calibration for the parameter K in the Two Wire Method

(c) Curing Conditions

Specimens were cured at room condition (temperature of 23±2˚C).

(d) Compression Test (ASTM C39)

The cylindrical specimen was capped and tested at a predetermined controlled displacement rate. The dimension of the specimen was measured using a Vernier caliper. In order to measure the strain, a commercially available extensiometer (accuracy of 0.001% strain) was used. The change in resistance was monitored using the two probe method and the parameter in Eqn. (2) was used relate the changes in resistivity to the applied stress.

(e) Physical Model

Laboratory models were designed and built at the University of Houston. The model was built to monitor the slurry level (drilling mud, spacer fluid and cement) during the installation and hardening of the cement. The observed resistance with time clearly indicated the level of slurry and to determine the depth at which the drilling fluid and cement was located. Several models were built separately and tested separately to demonstrate the real-time monitoring

The model was built using a flexi glass and metal pipe as shown in the Fig. 5 to simulate the formation and casing. The casing was instrumented with electrical wires to monitor the resistance change. The distance between two sensors was 4 to 6 inches and there were six levels of sensors as shown in the Fig. 5. Different combinations of the sensors were connected to a 300 Hz LCR device to measure resistance between those sensors. The horizontal electrical wire leads (sensors/monitors) are noted as a, b, c or d. The vertical wire leads are marked by 1 to 6. Figure 5 shows the different levels of liquid in the simulated well.

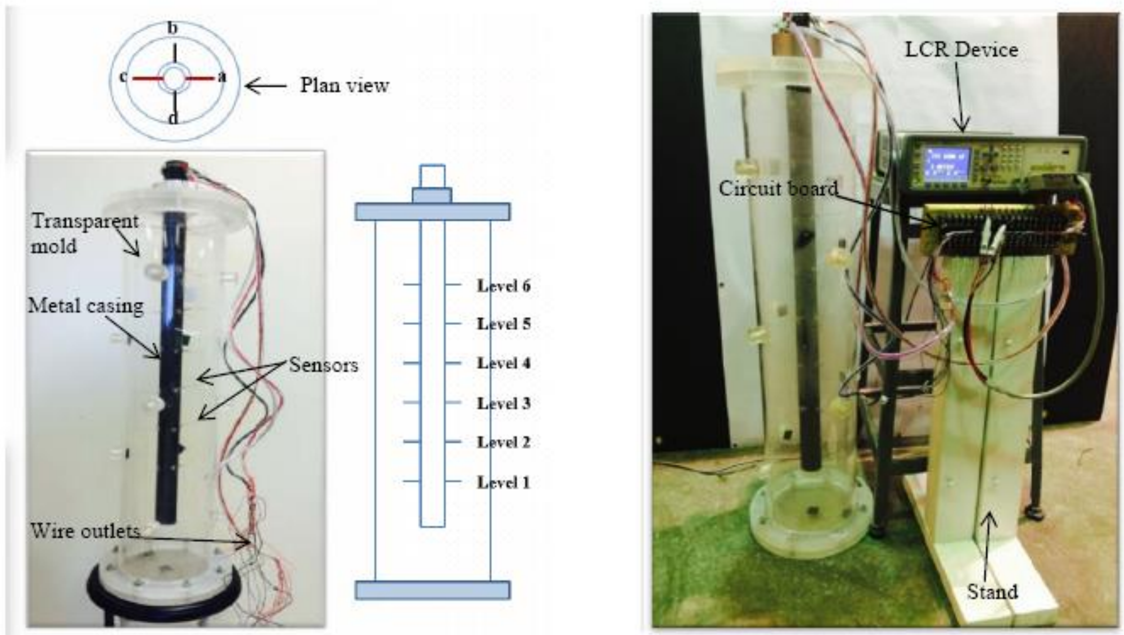

(a) Lab model (b) Monitoring System

Figure 5. Laboratory scale oil well model and monitoring system

4. Results and Discussion

The main focus of this study was to enhance the sensing capabilities of cement slurry from the time of mixing to solidified state. Also Class H and Class G oil well cements were used to demonstrate the potential of making the material more piezoresistive and sensing without significantly affecting the rheological properties. Although several modified cement slurries were studied only the performance of selected materials are presented. The test results form the unmodified cement was used as the baseline for comparison. Also various types of drilling muds were modified and tested to quantify the sensitivity of the changes.

4.1 Smart Cement

Electrical Resistivity

Based on the current study and past experience of the researchers, the change in resistivity with time can be represented as shown in Fig. 6. Hence, several parameters can be used in monitoring the curing (hardening process) of the cement. The parameters are initial resistivity (ρo), minimum resistivity (ρmin), time to reach the minimum resistivity (tmin), resistivity after 24 hours of curing ($\rho 24$), and percentage of maximum change in resistivity (Resistivity Index) [RI_{24hr}=($\frac{\rho 24-\rho min)}{\rho min}$]*100].

The test results from various smart cement compositions are summarized in Table 1. Fig. 7 illustrates the change in electrical resistivity (ρ) during curing time for modified smart cement using NanoFe. It was observed that all the curves of the different samples, with and without nanoFe, follow a similar trend with time. After initial mixing the electrical resistivity dropped to a minimum value (ρ_{min}), and then it gradually increased with time.

The decrease in electrical resistivity immediately after mixing was due to dissolution of soluble ions from the cement particles after cement was mixed with water, and the dissolving process of the ions caused the resistivity decrease during early period. Time to reach minimum resistivity, t_{min}, can be used as an index of speed of chemical reactions and cement set times. With the formation of resistive solid hydration products which block the conduction path, resistivity increased sharply with curing time. The following increase in electrical resistivity was caused by the formation of large amounts of hydration products in the cement matrix. Finally, a relatively stable increase in trend was reached by the ions' diffusion control of hydration process, and resistivity increased steadily for up to 24 hours, reaching a value of ρ_{24hr}. Change in electrical resistivity with respect to minimum resistivity quantifies the formation of solid hydration products, which leads to a decrease in porosity and, hence, the cement's strength development. Therefore, by tracking the change in resistivity of well cement, a clear understanding of hydration process and strength development can be obtained, which would be valuable in determining wait on cement (WOC) times. Variations of electrical resistivity with time for samples with different nanoFe content are summarized in Table 2.

The initial electrical resistivity (ρ_o) of smart cement with 0 percent, 0.5 percent and 1 percent of nanoFe were 1.06 Ω-m, 0.94 Ω-m and 0.87 Ω-m, a 11 percent and 18 percent reduction in the electrical resistivity when NanoFe concentration increased by 0.5 percent and 1 percent respectively as summarized in Table 1. Also the t_{min} was reduced by 5 percent and 11 percent when NanoFe concentration increased by 0.5 percent and 1 percent respectively as summarized in Table 3. The minimum resistivity (ρ_{min}) of smart cement with 0 percent, 0.5 percent and 1 percent of nanoFe were 0.9 Ω-m, 0.79 Ω-m and 0.65 Ω-m, a 12 percent and 28 percent reduction in the electrical resistivity when NanoFe concentration increased by 0.5 percent and 1 percent respectively as summarized in Table 3. The Resistivity index (RI_{24hr}) for smart cement with 0 percent, 0.5 percent and 1 percent of nanoFe were 333 percent, 335 percent and 346 percent respectively as summarized in Table 3. Change in RI_{24hr} increased with increasing the NanoFe content. These observed trends clearly indicate the sensitivity of resistivity to the changes occurring in the curing of cement (Table 1).

Modeling

Based on experimental results, model proposed by Mebarkia and Vipulanandan (1992) was modified to predict the electrical resistivity of smart cement during hydration up to 7 days of curing a shown in Fig. 7. The model is defined as follows:

$$\frac{1}{\rho} = \left(\frac{1}{\rho_{min}}\right)\left[\frac{\left(\frac{t+t_o}{t_{min}}\right)}{q+(1-p-q)*\left(\frac{t+t_o}{t_{min}}\right)+p*\left(\frac{t+t_o}{t_{min}}\right)^{\frac{q+p}{p}}}\right] \quad (8)$$

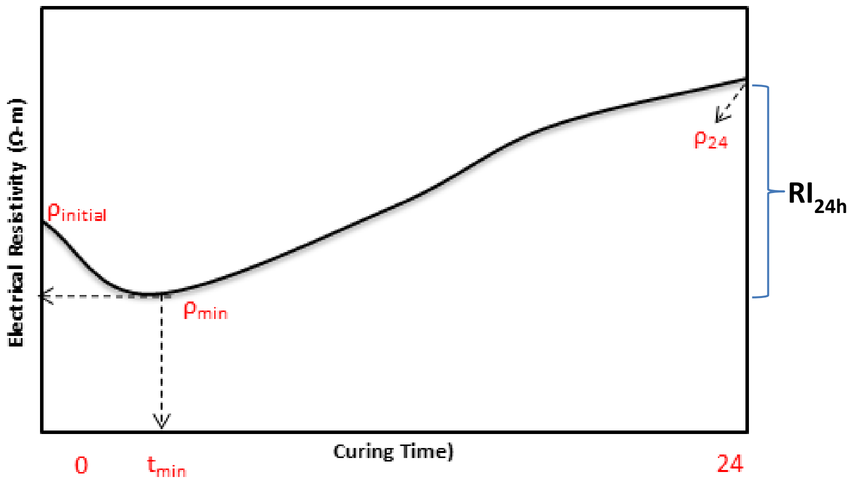

Figure 6. Typical bulk resistivity development with curing time

Where $\rho_{initial}$ is the initial electrical resistivity (Ω-m); ρ_{min}: minimum electrical resistivity (Ω-m); t_{min}: time corresponding minimum electrical resistivity (ρ_{min}); $p = (At + B)$, t_o; A, B, and q are model parameters; and t: time (minutes). As summarized in Table 2, model parameters t_o and B were sensitive to the NanoFe content and curing time. But parameter A was not influenced by the NanoFe content.

An addition of 1 percent NanoFe to the smart cement decreased the minimum resistivity (ρ_{min}) and minimum time (t_{min}) by 28 percent and 11 percent, respectively, as summarized in Table 3. Also, additions of 0.5 percent and 1 percent NanoFe to the smart cement reduced the electrical resistivity (ρ_{24}) of the smart cement by 12 percent and 28 percent, respectively, as shown in Table 1. Change in resistivity (Resistivity Index) (RI_{24hr}) increased with increasing the NanoFe content, e.g., adding 1 percent NanoFe to the smart cement caused the RI_{24hr} to increase by 10 percent, as summarized in Table 1.

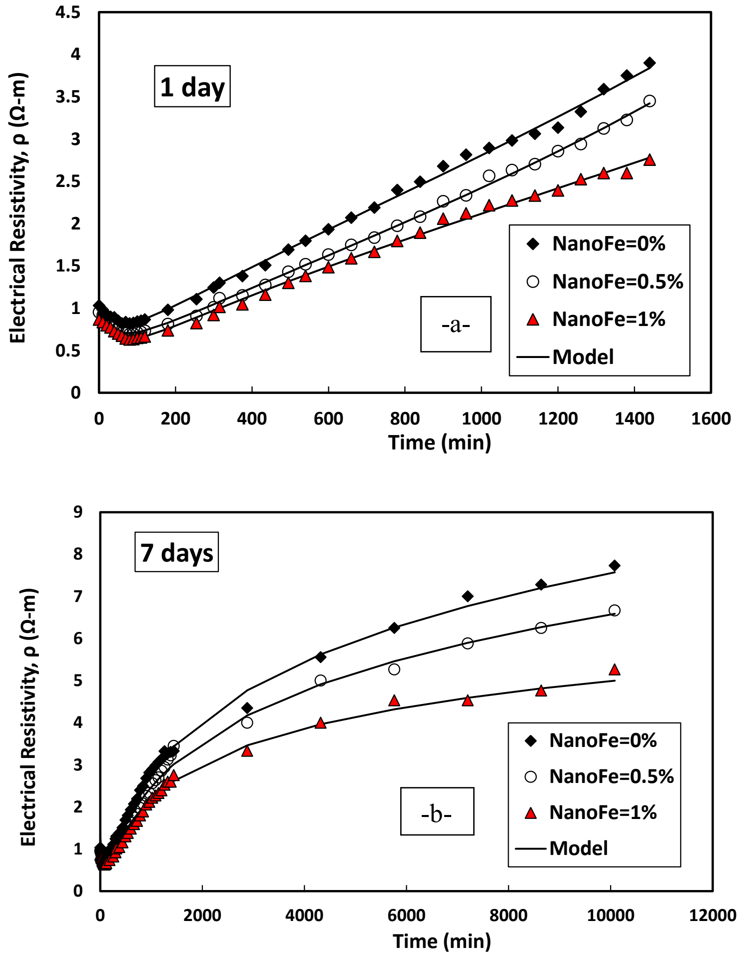

Figure 7. Bulk electrical resistivity development of smart cement with various amount of NanoFe: (a) 1 day and (b) 7 days

Table 1. Summary of bulk resistivity parameters for smart cement with various NanoFe content

NanoFe (%)	**Initial resistivity, ρ_o(Ω-m)**	**ρ_{min} (Ω-m)**	**t_{min} (min)**	**ρ_{24hr} (Ω-m)**	**$\rho_{7\ days}$ (Ω-m)**	**$RI_{24\ hr}$ (%)**	**$RI_{7\ days}$ (%)**
0	1.06	0.90	168	3.90	7.7	333	820
0.5	0.94	0.79	160	3.44	6.7	335	800
1	0.87	0.65	152	2.90	5.2	346	739

Table 2. Model parameters for electrical resistivity of smart cement with various NanoFe content

NanoFe (%)	Curing Time (day)	ρ_{min} (Ω.m)	t_{min} (min)	q	t_o (min)	A	B	RMSE (1/Ω.m)	R^2
0	1	0.90	168	0.69	60	-0.0001	2.38	0.034	0.99
0.5		0.79	160	0.65	55	-0.0001	2.21	0.036	0.98
1		0.65	152	0.58	50	-0.0001	1.83	0.042	0.97
0	7	0.90	168	2.18	73	-0.0001	6.60	0.071	0.99
0.5		0.79	160	0.70	70	-0.0001	4.80	0.070	0.95
1		0.65	152	0.67	68	-0.0001	2.94	0.025	0.99

Compressive Behavior

The compressive stress–piezoresistive behavior of cement is shown in Fig. 8. The piezoresistivity of the failure was 0.72 % and 54 % after one and 28 days curing.

(i) Nano Iron

Strength

Curing time

(i) 1 day: The average respective compressive strengths (σ_f) of the smart cements with 0 percent, 0.5 percent, and 1 percent NanoFe added after 1 day of curing were 1585 psi, 1694 psi, and 1995 psi, representing a 7 percent and 26 percent increase due to the addition of 0.5 percent and 1 percent NanoFe, respectively, as shown in Fig. 9.

(ii) 28 days: The average compressive strength of smart cement modified with 0 percent, 0.5 percent, and 1 percent NanoFe after 28 days of curing were 2810 psi, 3035 psi, and 4000 psi, respectively, representing an 8 percent and a 42 percent increase due to the addition of 0.5 percent and 1 percent NanoFe, respectively, as shown in Fig. 9.

Piezoresistivity

Curing time

(i) 1 day: The addition of 0.1 percent CF to the cement with w/c ratio of 0.38 increased the change in electrical resistivity of oil well cement at failure $\left(\frac{\Delta\rho}{\rho_o}\right)_f$ by 583 percent, as summarized in Table 3. The addition of 0.5 percent and 1 percent NanoFe to the smart cement after 1 day of curing increased the electrical resistivity at failure $\left(\frac{\Delta\rho}{\rho_o}\right)_f$ by 618 percent and 700 percent, respectively, as summarized in Table 3. The piezoresistivity at failure for 1 percent NanoFe was about 3500 times higher than the compressive strain at failure for the 0.2 percent NanoFe material sample.

(ii) 28 days: *The* addition of 0.1 percent CF to the cement with w/c ratio of 0.38 increased the change in electrical resistivity of oil well cement at failure $\left(\frac{\Delta\rho}{\rho_o}\right)_f$ by 400 percent, as summarized in Table 3. Adding 0.5 percent and 1 percent of NanoFe to the smart cement increased the electrical resistivity at failure $\left(\frac{\Delta\rho}{\rho_o}\right)_f$ to 452 percent and 574 percent, respectively, after 28 days of curing, as summarized in Table 5. The piezoresistivity at failure for 1 percent NanoFe was over 2800 times higher than the compressive strain at failure for the 0.2 percent NanoFe cement sample.

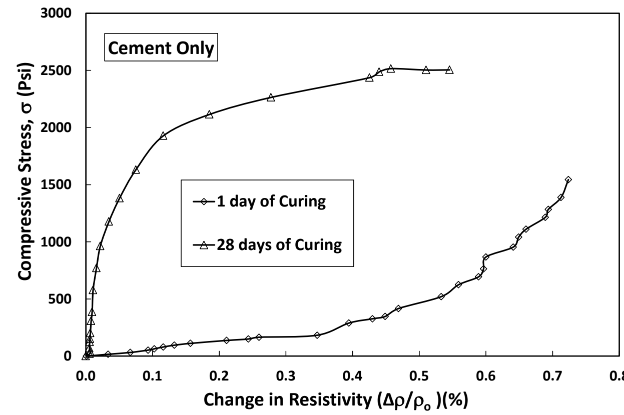

Figure 8: Piezoresistive behavior of oil well cement with curing time

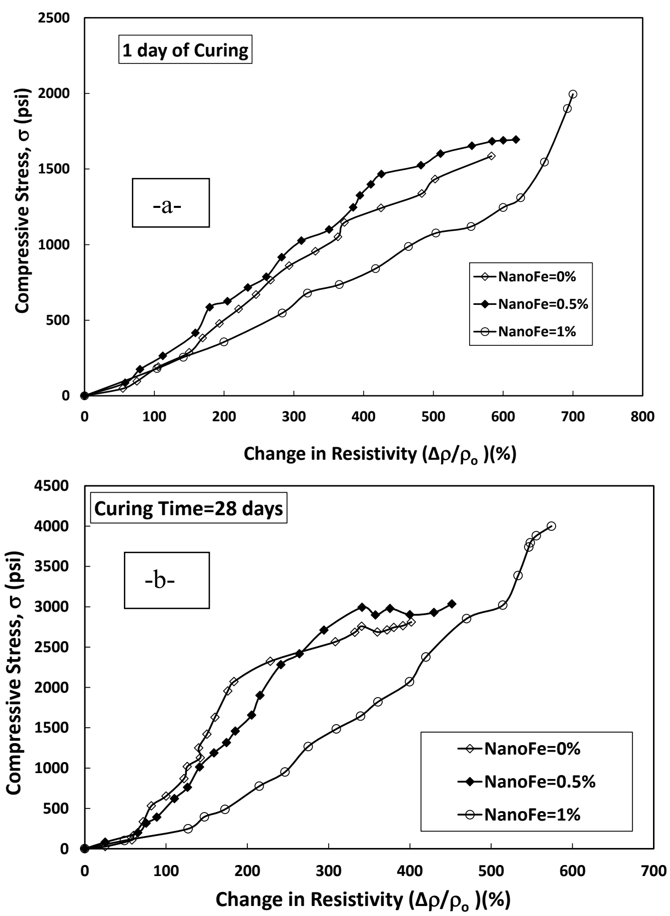

Figure 9. Piezoresistive behavior of smart cement modified with NanoFe after: (a) 1 day and (b) 28 days of curing time

Table 3. Summary of change in electrical resistivity and strength for smart cement modified with NanoFe content

Material	Additive (%)	Curing Time (day)	$\left(\frac{\Delta\rho}{\rho_o}\right)_f$ (%)	σ_f (psi)
Cement Only	-	1	0.70	1537
		28	0.55	2509
Cement (Smart Cement)	0.1% CF	1	583	1585
		28	402	2810
Smart Cement	0.5% NanoFe	1	618	1694
		28	452	3035
Smart Cement	1% NanoFe	1	700	1995
		28	574	4000

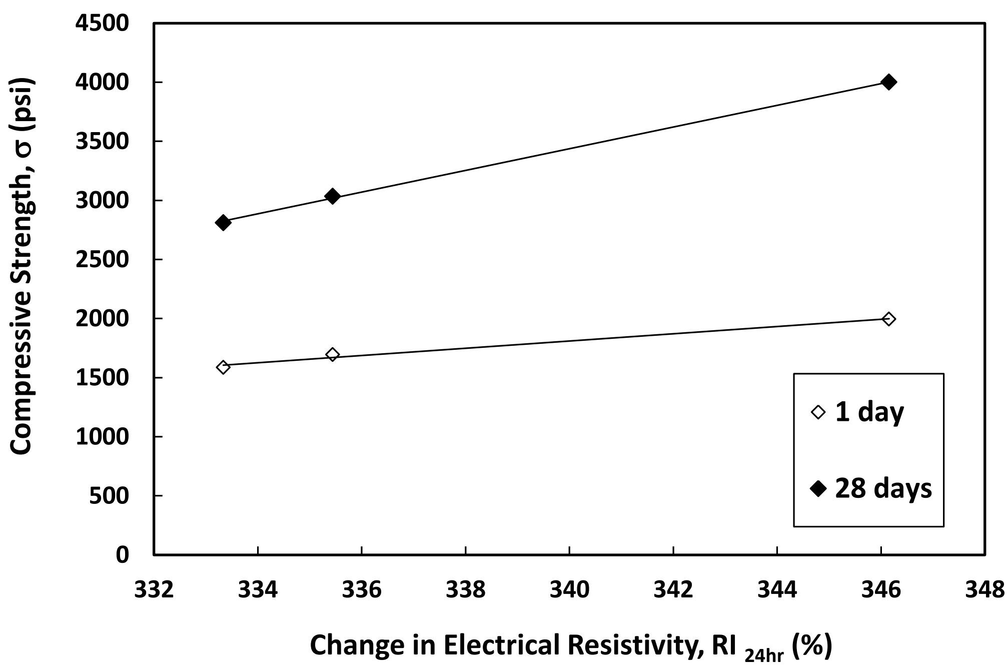

Figure 10. Relationship between resistivity index ($RI_{24\ hr}$) and compressive strength of smart cement modified with NanoFe

Compressive Strength – Resistivity Relationship

During the entire cement hydration process both the electrical resistivity and compressive strength of the cement increased gradually with the curing time. For cement pastes with various NanoFe content, the change in resistivity was varied during the hardening. The cement paste without NanoFe had the lowest electrical resistivity change (RI_{24hr}), as summarized in Table 2.

The relationships between (RI_{24hr}) and the 1 day and 28 day compressive strengths (psi) (Fig. 10) were as follows:

$$\sigma_{1day} = 31 \times RI_{24hr} - 8636 \quad R^2=0.98 \tag{9}$$

$$\sigma_{28days} = 92 \times RI_{24hr} - 27817 \quad R^2=0.99 \tag{10}$$

(ii) Nano Calcium Carbonate (NCC)

1 day curing

(a) Smart Cement: As shown in Fig.11, after 1 day of curing, the piezoresistivity of the smart cement was 375%. Parameters *p* and *q* for the model were 0.15 and 0.57 respectively.

(b) NCC Modified Smart Cement: Adding 1% of NCC enhanced the piezoresistivity by 37% which leads to have 514% piezoresistivity after 1 day of curing. This enhancement in piezoresistivity is due to microstructure enhancement of the smart cement. This enhancement is well enough to reduce the effect of contamination on the piezoresistivity behavior of the smart cement.

(c) Contaminated Smart Cement: As shown in Fig.12, contamination of the smart cement with OBM reduced the piezoresistive behavior of the cement considerably. 3% of OBM contamination with smart cement reduced the piezoresistivity to 231%, a 38% decrease.

(d) Contaminated NCC Modified Smart Cement: Adding 1% of NCC caused the piezoresistivity of the contaminated cement with 3% of OBM enhanced by 38% to 319% piezoresistivity after 1 day of curing under water. This increasing in piezoresistivity is due to enhancement in the microstructure of the smart cement with adding 1% of NCC.

28 days curing

(a) Smart Cement: As shown in Fig.12, after 28 days of curing, the piezoresistivity of the smart cement was 204%.

(b) NCC Modified Smart Cement: Adding 1% of NCC caused enhancement in piezoresistivity by 28% which leads to have 260% piezoresistivity after 28 days of curing under water. This enhancement in piezoresistivity is due to microstructure enhancement of the smart cement.

(c) Contaminated Smart Cement: As shown in Fig.13, 3% of OBM contamination reduced the piezoresistivity of the smart cement to 154%, a 25% decrease.

(d) Contaminated NCC Modified Smart Cement: Adding 1% of NCC caused the piezoresistivity of the contaminated cement with 3% of OBM enhanced by 45% to 221% after 28 days of curing under water.

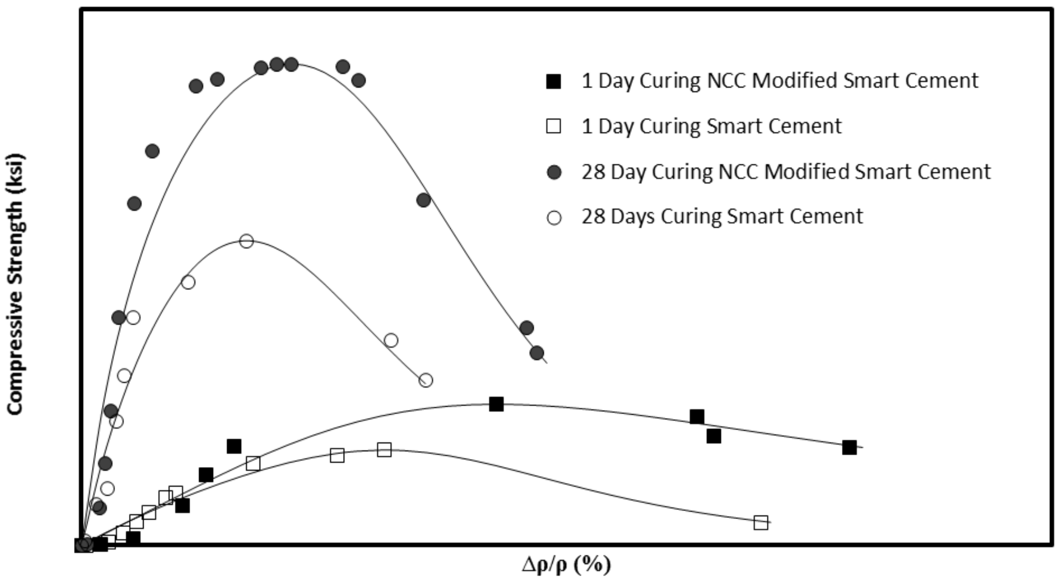

Figure 11. Piezoresistive behavior of the smart cement with and without 1% of NCC modification after 1 and 28 days of curing

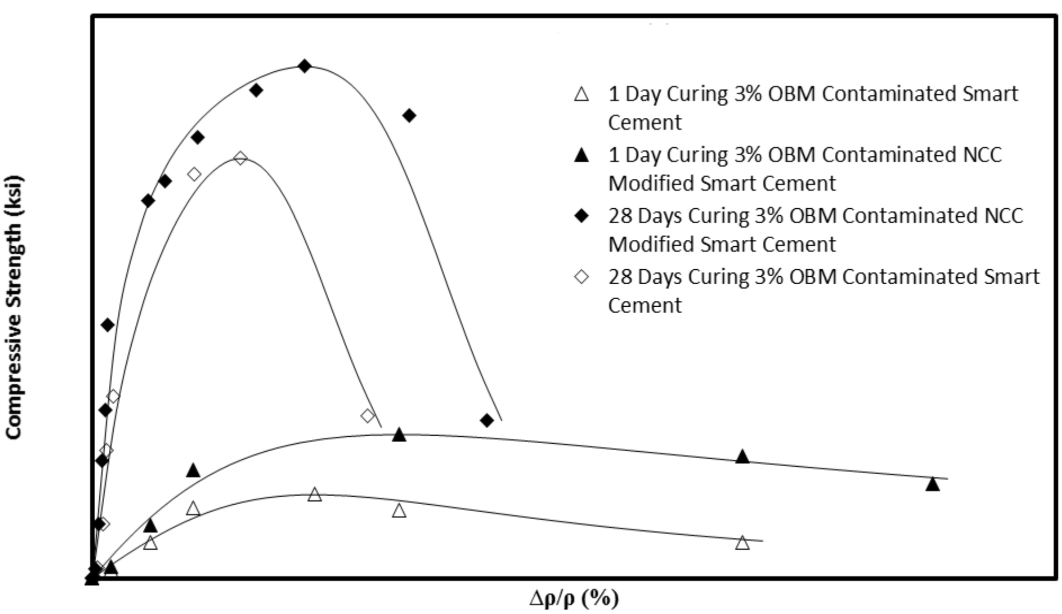

Figure 12. Piezoresistivity behavior of the 3% OBM contaminated smart cement with and without 1% of NCC modification after 1 and 28 days of curing

Model Study: Monitoring the Cement Slurry Level

The smart cement slurry rise and the vertical resistances are reported in Figure 13. Similar pattern to water rise was observed which enabled the sensing method to detect the level of the cement slurry.

In contrast to 1000 Ω resistance of the drilling mud (water) the rage of resistance of cement slurry was in the range of 20 to 50 Ω for the time interval monitored. This observation showed that the material can be distinguished based on the resistance value while identifying the level of the slurry.

Curing of Cement Sheath

Resistivity of the smart cement

The Resistivity of the cement slurry with curing time of up to 100 days was determined using the smart cement slurry samples (2 inches diameter and 4 inches height cylindrical mold) that was used for the small model study. The resistivity increased with curing time under the curing of room temperature and humidity (Figure 14).

Predicted (Electrical Resistance Model –ERM) and measured resistance for hardening cement

Using the parameters K and the resistivity-time relationship (Fig. 13), the changes in the cement sheath resistance in the small model was predicted using the relationship in Eqn. (1). Figures 15 through Figure 19 show the variations of the predicted resistance value and also the actual measured values for different wire setup/combinations.

Vertical resistance

Wire setup-a

For the wire setup-a, the wire combination a1-a2 showed that the predicted values were lower than the measured values up to 14 days of curing but after that the measured resistance values were in the range of the predicted resistance (Figure 14). This may be because in the small model#2 the cement is hydrating under pressure and temperature and the resistivity used (Fig. 13) to predict the resistance was cured under room condition under no pressure.

For wire setup-a wire combination a1 and a4, the measured values were very close to the predicted values (Figure 15). The wire at level a4 is very close to the surface of the small model which showed very similar hydration to the test sample (Fig. 13). The measure resistance values matched very well with the predicted values.

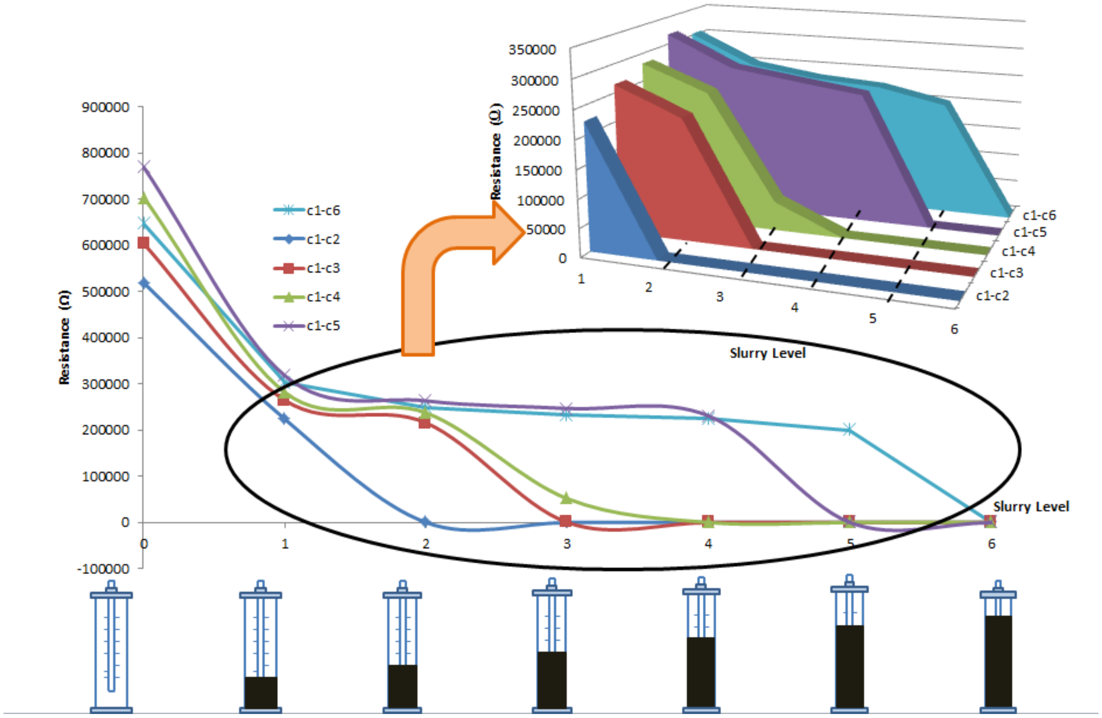

Figure 13. Variation of vertical resistance with different level of cement slurry

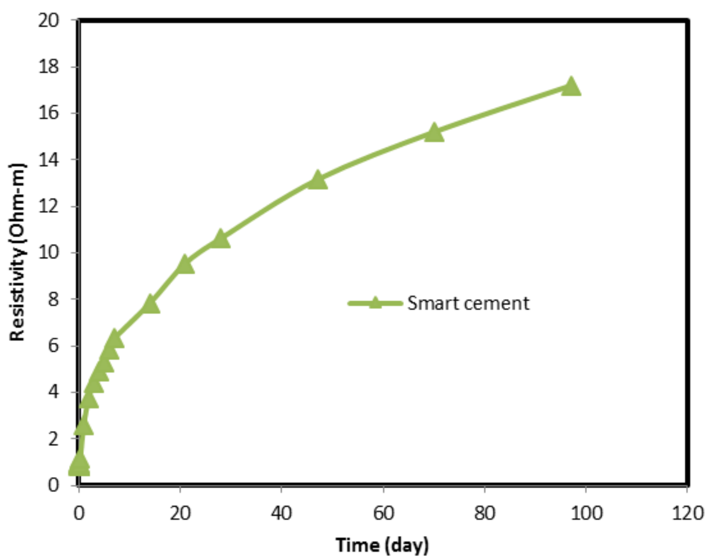

Figure 14. Variation of smart cement resistivity with curing time for samples cured under room conditions (23ºC and 50% relative humidity (RH))

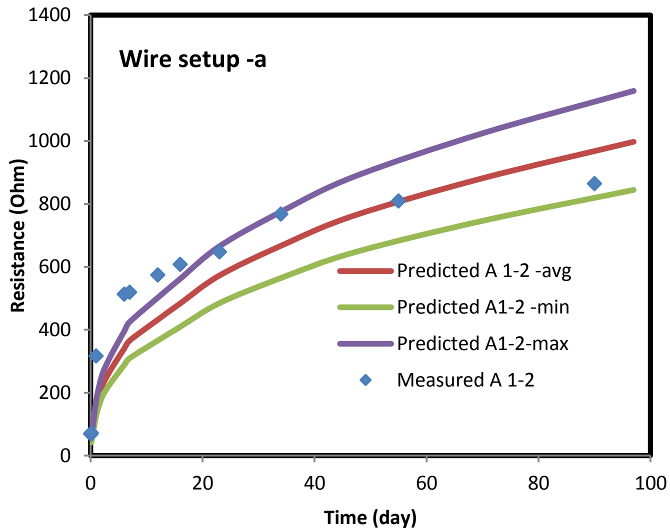

Figure 15. Comparing the predicted and measured resistance for wire setup-a for wire combination a1-a2.

Pressure Test

Air pressure (P_i) was applied inside the casing to load the cement-sheath and the electrical resistance (R_o in Ohms) was measured between Level 1-2, Level 2-3, Level 3-4, Level 4-5, were monitored while the air pressure was applied inside the casing (Figure 16).

Case 1: Initial Condition (No pressure, Pi = 0)

The initial resistance was higher at the bottom (level 1-2) due to weight of the cement sheath and was lower at the top level (level 4-5). The electrical resistance increased with the depth and varied from 400 to 800 ohms. This is partly due to the piezoresistive property of the smart cement, where the electrical resistance will be higher with increase in pressure with depth.

Case 2: Pi = 60 psi

Internal pressure of 60 psi was applied and the resistance changes were measured after 26 hours. The change in resistance was normalized with initial resistance $\Delta R/R(\%)$ is shown in Figure 17. The resistivity change in the smart cement due to the applied pressure was about 0.5 to 0.6%, indicating the piezoresistivity of the smart cement.

Case 3: Pi = 100 psi

Pressure of 100 psi was applied and the resistance changes were measured in 26 hours and reported in the form of $\Delta R/R$ (%) in Figure 17. The resistivity change in the smart cement due to the applied pressure of 100 psi was about 2.5%, indicating the piezoresistivity of the smart cement.

Case 3: Pi = 140 psi

Internal pressure of 140 psi was applied and the resistance changes were measured in 26 hours and reported in the form of ΔR/R in Fig. 17. The resistivity change in the smart cement due to the applied pressure was about 6.5 to 7%, indicating the piezoresitivity of the smart cement.

Piezoresistive Modeling

The stress at every point can be separated into mean stress and deviatoric stress. The change in the deviatoric stress due to the applied pressure (P_i) along the axis of the casing (z-axis) is represented as ΔS_{zz}. Using equilibrium and stress analyses, it can be shown that ΔS_{zz} is directly proportional to the applied internal pressure P_i. Hence the change in deviatoric stress can be represented as follows:

$$\Delta S_{zz} = f(Pi) \tag{5}$$

The variation of internal applied pressure with the resistivity of smart cement ($\Delta\rho/\rho_o$) is shown in Fig. 18, and the response of the smart cement is nonlinear.

p, q model

The nonlinear p-q model was developed by Vipulanandan et al. (1990) and was used to predict $\Delta\rho_z/\rho_z$ variation with the applied pressure. The relationship can be represented as follows:

$$P_i = \frac{(\frac{\Delta\rho_z}{\rho_z})}{q+(1-q-p)(\frac{\Delta\rho_z}{\rho_z})+p(\frac{\Delta\rho_z}{\rho_z})^{\frac{p+q}{p}}} \tag{6}$$

The model parameters p and q were 1.2 and 3 respectively. Hence measuring the change resistivity of the smart cement it will be possible to predict the pressure in the casing and also the stress in the cement sheath.

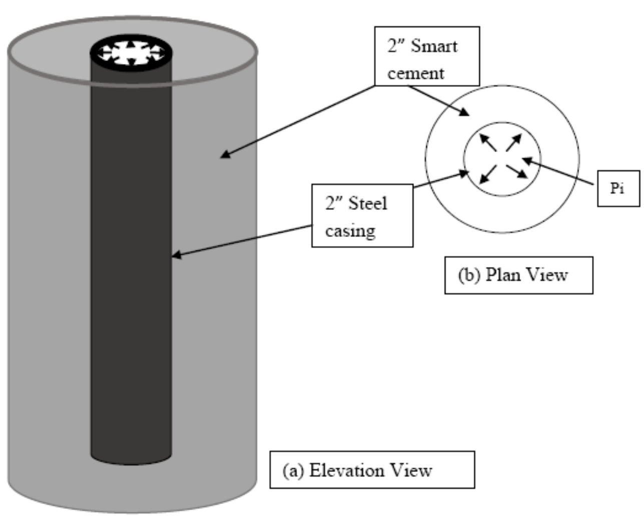

Figure 17. The configuration of the pressure applied in the inside the steel casing

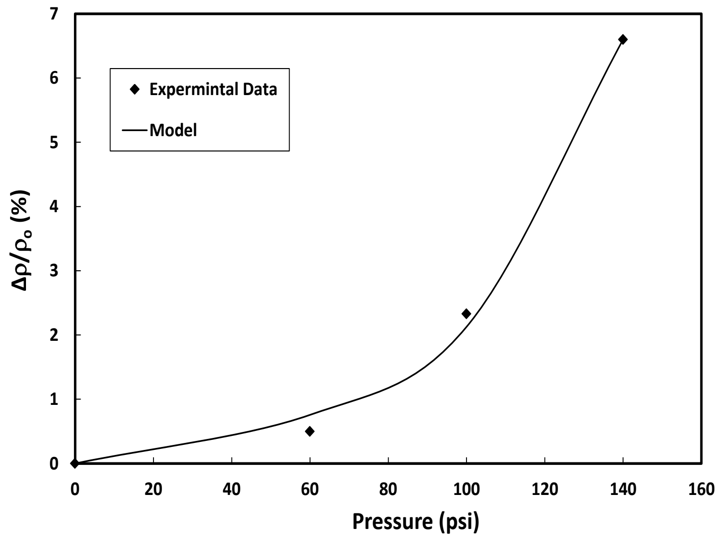

Figure 18. Model prediction of changes in resistivity with applied pressure for smart cement after 100 days of curing.

5. Conclusions

Based on experimental and analytical study on smart cement modified with nanoparticles (NanoFe and nano calcium carbonate) up to 1 percent and the physical model test, the following conclusions are advanced:

1. Resistivity was sensitive to the amount of NanoFe used to modified smart cement. The amount of NanoFe can be detected based on the change in the initial resistivity. An addition of 1 percent NanoFe decreased the initial electrical resistivity (ρ_o) of smart cement by 32 percent and reduced the time to reach minimum resistivity by 10 minutes. The maximum change in resistance within the first 24 hours of curing increased from 307 percent to 338 percent.

2. Modifying Class H cement with NanoFe material resulted in cement with increased viscosity and yield stress. A newly developed hyperbolic model predicted the shear-thinning behavior of smart cement which had been modified with NanoFe.

3. The initial resistivity of up to 1 percent of nanoFe modified smart cement exhibited an increase by more than 32 percent. Initial electrical resistivity can be used as a good indicator for quality control.

4. The resistivity index (RI_{24hr}) of the smart cement without nanoFe (i.e., lower strength) was higher than that of the smart cement with 1 percent nanoFe (higher strength). A linear correlation was found between resistivity index and compressive strength at different curing ages.

5. NCC modification resulted in considerable improvement of compressive strength and piezoresistivy of OBM contaminated smart cement both after 1 and 28 days of curing under water.

6. Using the laboratory model it was possible to demonstrate the real-time monitoring of the well bore with drilling mud, space fluid and smart cement slurry.
7. Using the concept developed in this study, it is possible to use the K parameter and predict the changes in the resistance of drilling and hardening smart cement.
8. Using a nonlinear model the change in electrical resistivity of smart cement was related to the applied pressure in the casing. The smart cement was very sensitive to the applied pressure

6. Acknowledgement

This study was supported by CIGMAT with funding from DOE/NETL/RPSEA (Project 10121-4501-01).

7. Bibliography

1. API Recommended Practice 10B (1997), Recommended Practice for Testing Well Cements Exploration and Production Department, 22^{nd} Edition.
2. API recommended Practice 65 (2002) Cementing Shallow Water Flow Zones in Deepwater Wells.
3. Carter, K. M. and Oort, E. (2014), Improved Regulatory Oversight Using Real- Time Data Monitoring Technologies in the Wake of Mocondo, SPE 170323, pp. 1-51.
4. Dom, P. B., S. Rabke, et al. (2007). "Development, verification, and improvement of a sediment-toxicity test for regulatory compliance." SPE Drilling & Completion, Vol. 22(2), 90-97.
5. Griffith, J. and Faul, R. (1997) "Mud Management Special Slurries Improve Deepwater Cementing Operations," Oil and Gas Journal, Vol. 95, No. 42, pp. 49-51.
6. Izon, D. and M. Mayes, M. (2007) "Absence of fatalities in blowouts encouraging in MMS study of OCS incidents 1992-2006," Well Control Magazine, pp. 86-90.
7. John B., (1992). "Class G and H Basic Oil Well Cements," World Cement.
8. Kim, J and Vipulanandan, C. (2006)"Removal of Lead from Contaminated Water and Clay Soil Using a Biosurfactant," Journal of Environmental Engineering, Vol. 132, No. 7, pp.857-865.
9. Kim, J. and Vipulanandan, C. (2003) "Effect of pH, Sulfate and Sodium on the EDTA titration of Calcium," Cement and Concrete Research, Vol. 33(5), pp. 621-627.
10. Kyle, M. and Van Eric (2014), Improved regulatory oversight using real- time data monitoring technologies in the Wake of Mocondo, SPE 170323, pp. 1-51.
11. Li, F., Vipulanandan, C. and Mohanty, K. (2003) "Microemulsion and Solution Approaches to Nanoparticle Iron Production for Degradation of Trichloroethylene,"

Colloids and Surfaces A: Physicochemical and Engineering Aspects, Vol. 223, No. 1, pp. 103-112.

12. Labibzadeh, M., Zhhabizadeh, B. and Khajehdezfuly, A., (2010) "Early Age Compressive Strength Assessment of Oil Well Class G Cement Due to Borehole Pressure and Temperature Changes, Journal of American Science, Vol. 6, No.7, pp.38-47.

13. Nam, M. S. and Vipulanandan, C. (2008) "Roughness and Unit Side Resistances of Drilled Shafts Socketed in Clay Shale and Limestone, Journal of Geotechnical and Geoenvironmental Engineering, Vol. 134, No. 9 , pp. 1272-1279.

14. Miranda C.R., Carvalho K.T., Vargas A.A., Rodrigues L.F., Marchesini F.H. (2007). “Minimizing fluid contamination during oil well cementing operations”; OMC 2007

15. Mirza, J. et al. (2002) "Basic Rheological and mechanical properties of High Volume Fly Ash Grouts," Construction and Building Materials, Vol. 16, pp.353-363.

16. Ozgurel, G., Gonzalez, H. A. and Vipulanandan, C., (2005) "Two dimensional Model Study on Infiltration Control at a Lateral Pipe Joint using Acrylamide Grout", Proceedings, Pipelines 2005, ASCE, pp. 631-642.

17. Park, J., Vipulanandan, C., Kim, J. and Oh, M. H. (2006) "Effect of Surfactants and Electrolyte Solutions on the Properties of Soils," Journal of Environmental Geology, Vol. 49, pp.977-989.

18. Ravi, K. et al. (2007) "Comparative Study of mechanical Properties of Density-reduced Cement Compositions, SPE Drilling & Completion, Vol. 22, No. 2, pp. 119-126.

19. Ramachandran, V. S. (1984) Concrete Admixture Handbook, Noyes Publication, Park Ridge, New Jersey, 628 pp.

20. Samsuri A., Junin R., Osman A.M. (2001). The utilization of Malaysian local bentonite as an extender and free water controller in oil-well cement technology, Society of Petroleum Engineers. Doi: 10.2118/68674-MS.

21. Sarap G.D., Sivanandan M., Patil S., Deshpande A.P. (2009) The use of high performance spacers for zonal isolation in high temperature High-pressure wells SPE/IADC 124275.

22. Thaemlitz, J., A. D. Patel, et al. (1999). "New environmentally safe high-temperature water-based drilling-fluid system." SPE Drilling & Completion Vol. 14(3), 185-189.

23. Vipulanandan, C. and Leung, M., (1991)" Seepage Control in Contaminated and Permeable Houston Clay: Laboratory Study," Hazardous Waste & Hazardous Materials, Vol. 8, No. 1, 17-32.

24. Vipulanandan, C. and Neelam Kumar, M.(2000) "Properties of Fly Ash-Cement Cellular Grouts for Sliplining and Backfilling Applications," Proceedings, Advances in Grouting and Ground Modification, ASCE, GSP 104, Denver, CO, pp. 200-214.

25. Vipulanandan, C., and Sett, K. (2004) "Development and Characterization of Piezoresistive Smart Structural Materials", Proceedings, Engineering, Construction and Operations in Challenging Environments, Earth & Space 2004, ASCE Aerospace Division, League City, TX, pp. 656-663.

26. Vipulanandan, C., and Liu, J. (2005) "Polyuretane Based Grouts for Deep Off-Shore Pipe-in-Pipe Application", Proceedings, Pipelines 2005, ASCE, Houston, TX, pp. 216-227.

27. Vipulanandan, C., and Garas, V. (2006), "Piezoresistivity of Carbon Fiber Reinforced Cement Mortar", Proceedings, Engineering, Construction and Operations in Challenging Environments, Earth & Space 2006, Proceedings ASCE Aerospace Division, League City, TX, CD-ROM.

28. Vipulanandan, C. and Mamidi, B. (2008),"Biosurfactant Flushing of PCE Contaminated Clayey Soils," Proceedings, GeoCongress 2008, Geotechnics of Waste Management and Remediation, ASCE, GSP 177, pp. 495-502.

29. Vipulanandan, C. and Nam, E. (2009), "Drilled Shaft Socketed in Uncemented Clay Shale," Proceedings, Foundation Congress 2009, Contemporary Topics in Deep Foundations, ASCE, GSP 185, pp. 151-158.

30. Vipulanandan, C. and Usluogullari, O. (2009), "Field Evaluation of A New Down-Hole Penetrometer" Proceedings, Contemporary Topics in In Situ Testing, Analysis, and Reliability of Foundations, Foundation Congress 2009, ASCE, GSP 186, pp. 119-126.

31. Vipulanandan, C., Dimrican, E. and Harendra, S. (2010) "Artificial Neural Network and Nonlinear Models for Gelling and Maximum Curing Temperature Rise in Polymer Grouts," Journal of Materials in Civil Engineering, Volume 23, No. 4, p. 1-6.

32. Vipulanandan, C. and Prasanth, P., (2013)" Impedance Spectroscopy Characterization of a piezoresistive Structural Polymer Composite Bulk Sensor," Journal of Testing and Evaluation, Vol. 41, No.6, 898-904.

33. Vipulanandan et al. (2014) "Development and Characterization of Smart Cement for Real Time Monitoring of Ultra-Deepwater Oil Well Cementing Applications, OTC-25099-MS.

34. Vipulanandan et al. (2014) "Characterization of Smart Cement Modified with Sodium Meta Silicate for Ultra-Deepwater Oil Well Cementing Applications, AADE-2014.

35. Vipulanandan, C. Heidari, M., Qu, Q., Farzam, H., and Pappas, J. M. (2014), “Behaviour of piezoresistive smart cement contaminated with oil based drilling mud,” Offshore Technology Conference, OTC 25200-MS, pp. 1-14.

36. C. Vipulanandan, C. and A. Mohammed, A. (2014), “Hyperbolic rheological model with shear stress limit for acrylamide polymer modified bentonite drilling muds,” Journal of Petroleum Science and Engineering, 122 (2014) 38–47.

37. Wang, S. Y. and Vipulanandan, C., (1996) "Leachability of Lead From Solidified Cement-Fly Ash Binders," Cement and Concrete Research, Vol. 26, No. 6, pp. 895-905.

38. Zhang M., Sisomphon K., Ng T.S, and Sun D.J, (2010). “Effect of superplasticizers on workability retention and initial setting time of cement pastes,” Construction and Building Materials 24, 1700–1707.

39. Zhang J., Weissinger E.A, Peethamparan S, and Scherer G.W., (2010). “Early hydration and setting of oil well cement,” Cement and Concrete research, Vol. 40, 1023-1033.